Acta Crystallographica Section B
Structural Science
ISSN 0108-7681

On the sequence of three related phases of $[Ni(H_2O)_2(15\text{-crown-}5)](HSO_4)_2$ in the temperature range 110–295 K

Maxime A. Siegler[a,b]* and Eli Stavitski[c]

[a]Crystal and Structural Chemistry, Bijvoet Center for Biomolecular Research, Faculty of Science, Utrecht University, Padualaan 8, 3584 CH Utrecht, The Netherlands, [b]Department of Chemistry, The Johns Hopkins University, Baltimore, Maryland 21218, USA, and [c]Inorganic Chemistry and Catalysis Group, Department of Chemistry, Utrecht University, Sorbonnelaan 16, 3584 CA Utrecht, The Netherlands

Correspondence e-mail: xray@jhu.edu

Received 27 January 2010
Accepted 28 May 2010

Attempts to prepare the compound $[Ni(H_2O)_2(15\text{-crown-}5)](X)_2$ were eventually successful with $X = NO_3^-$ provided that a synthetic route aimed at restricting water was followed. Application of this method was extended to make the analogous compound with $X = HSO_4^-$, for which three symmetry-related phases were isolated between 295 and 110 K: a room-temperature phase with $Z' = \frac{1}{2}$ [phase (I)], an intermediate-temperature phase with $Z' = 1$ [phase (II)] and a low-temperature phase with $Z' = 2$ [phase (III)]. The phases are related by two reversible solid–solid phase transitions, and both transitions take place without a significant loss of crystallinity. In the phase sequence (I) $\leftrightarrow$ (II) $\leftrightarrow$ (III) (Z': $\frac{1}{2} \leftrightarrow 1 \leftrightarrow 2$), the crystal packing remains remarkably similar but the degree of order in the crystal changes significantly; the structure is very disordered at room and intermediate temperatures but is ordered at 110 K. The compound $[Ni(H_2O)_2(15\text{-crown-}5)](HSO_4)_2$ has a complicated hydrogen-bonding network, which contains O—H···O bonds between the counterions. Structural changes are largest along some face-diagonal directions in the sequence (I) $\leftrightarrow$ (II) $\leftrightarrow$ (III).

1. Introduction

In a series of three papers (Hao, Parkin & Brock, 2005; Hao, Siegler *et al.*, 2005; Siegler, Hao *et al.*, 2008), Brock and co-workers have examined thoroughly the structural family $[M(H_2O)_2(15\text{-crown-}5)](NO_3)_2$ (M = Mg, Mn, Fe, Co, Ni, Cu and Zn). This family was classified into two subgroups that include phases with either a two-dimensional (M = Mg, Mn, Fe, Ni, Cu and Zn) or a three-dimensional (M = Mn and Co) hydrogen-bonded network. In the two-dimensional subgroup, each of the compounds has one reversible solid–solid phase transition and two phases in the temperature range 90—315 K. All of the two-dimensional phases are structural variants in the modulation of the same basic structure, and the Z' number (*i.e.* the number of independent formula units in the asymmetric unit) may take the values 2, 3, 5 and 8.

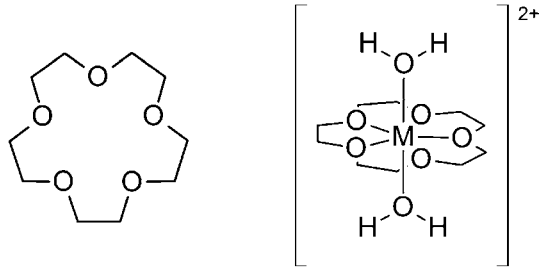

15C5 $[M(H_2O)_2(15C5)]^{2+}$

The case of M = Ni is special because the insertion of the metal ion into the cavity of the 15-crown-5 ligand (hereafter 15C5) does not take place *via* the 'normal' synthetic route used for M = Mg, Mn, Fe, Co, Cu and Zn; structural disorder of the metal ion has also been exclusively found for the Ni compound (Siegler, Parkin *et al.*, 2008). While attempts were made to synthesize $[Ni(H_2O)_2(15C5)](NO_3)_2$, six other compounds containing hexa-coordinated Ni^{2+} ions (with at least two axial water ligands), nitrate ions, uncoordinated 15C5 molecules and sometimes uncoordinated solvent molecules (*e.g.* water and acetonitrile) were synthesized. All have in common the $\cdots$15C5$\cdots$H$_2$O—Ni—OH$_2\cdots$15C5$\cdots$ hydrogen-bonded motif, but the H_2O:Ni^{2+} ratios can vary from 8:1 to 2:1. Discoveries of subtle sequences of symmetry-related structures for three of these compounds, *i.e.* $[Ni(H_2O)_2(MeCN)(NO_3)_2]\cdot$15C5$\cdot$MeCN (hereafter the acetonitrile compound), $[Ni(H_2O)_6](NO_3)_2\cdot$15C5$\cdot 2H_2O$ and the first polymorph of $[Ni(H_2O)_6](NO_3)_2\cdot$15C5$\cdot H_2O$ (hereafter the dihydrate and monohydrate compounds), were serendipitous. These sequences are characterized by an increase of the Z' number in the temperature-descending regimen (but sometimes there is an intermediate phase with Z' as unusually large as 5 and 7; these very high Z' phases are likely to be approximations to incommensurate modulated phases); Z': $\frac{1}{2} \Rightarrow 5 \Rightarrow 1 \Rightarrow 2$ (acetonitrile); Z': $\frac{1}{4} \Rightarrow \frac{1}{2} \Rightarrow 7 \Rightarrow 1$ (dihydrate) and Z': $1 \Rightarrow 2$ (monohydrate) from 298 to 90 K. Further details about these systems can be found in Chapters 4, 5 and 6 of Maxime A. Siegler's dissertation (Siegler, 2007). The individual phase sequences will be reported in separate papers (Siegler, Hao *et al.*, 2010; Siegler, Parkin & Brock, 2010).

The initial motivation of this research was to synthesize $[Ni(H_2O)_6](SO_4)\cdot$15C5$\cdot x$H$_2$O and $[Ni(H_2O)_6](HSO_4)_2\cdot$15C5$\cdot xH_2$O ($x$ = integer or half integer) compounds based on the common $\cdots$15C5$\cdots$H$_2$O—Ni—OH$_2\cdots$15C5$\cdots$ synthon; this synthon might be expected to induce some structural complexity in the solid state (*e.g.* structures with $Z' > 1$; Siegler, Parkin *et al.*, 2008). More phase sequences were expected, however, failure to make these two compounds eventually led to the synthesis of the compound $[Ni(H_2O)_2(15C5)](HSO_4)_2$ [hereafter (1)]. Previous experience with the analogous compound $[Ni(H_2O)_2(15C5)](NO_3)_2$ showed that the insertion of the Ni^{2+} ion into the cavity of the crown ether is challenging because the exchange of four strongly bonded water ligands of $[Ni(H_2O)_6]^{2+}$ for the more weakly bonded 15C5 ligand is not thermodynamically and kinetically favorable unless water is restricted throughout the synthesis (Siegler, Parkin *et al.*, 2008). A similar synthetic procedure was carried out in order to obtain crystals of $[Ni(H_2O)_2(15C5)](HSO_4)_2$.

The counterion replacement $NO_3^- \Rightarrow HSO_4^-$ raises important questions when structural comparisons between the two systems $[Ni(H_2O)_2(15C5)](X)_2$, X = NO_3^-, HSO_4^- are being considered:

(i) Based on the ability of the hydrogen sulfate counterions to form hydrogen-bonding interactions, what would be the influence of these interactions on the resulting crystal packing of (1)?

(ii) Would the metal coordination in $[Ni(H_2O)_2(15C5)]^{2+}$ be similar for the two compounds?

(iii) The two-dimensional structural family $[M(H_2O)_2(15C5)](NO_3)_2$ (M = Mg, Mn, Fe, Ni, Cu and Zn) includes many related phases having $Z' > 1$, would this trend be observed for (1)?

As a preliminary approach for this investigation, a search of the November 2009 version (5.31 + updates through February 2010) of the Cambridge Structural Database (Allen, 2002; hereafter the CSD) was made for structures containing M^{II}(15C5) [M^{II} = any divalent metal center coordinated by the O_{crown} atoms of the crown ether] and hydrogen sulfate counterions. The search gave only two entries, which correspond to the compounds $[M(H_2O)_2(15C5)](HSO_4)_2$, M = Mn and Cd (Braga *et al.*, 2007; refcodes SIDKEW and SIDKIA). The two structures are isomorphous and have $Z' = \frac{1}{2}$ at room temperature. Both structures have been reported as partly ordered because the counterions are disordered. Some structural problems were nonetheless overlooked: the cations $[M(H_2O)_2(15C5)]^{2+}$ (M = Mn, Cd), which are found at sites of statistical mirror symmetry, were treated as ordered although the 15-crown-5 ligand has no mirror symmetry. The eccentric ellipsoids for some of the C_{crown} atoms, which are very elongated along the direction perpendicular to the mean molecular plane of the crown ether, and the unusually short C—C bond lengths [*e.g.* 1.297 (15) and 1.29 (3) Å for SIDKEW and SIDKIA] were strong warning signs suggesting disorder of the 15-crown-5 ligand.[1] In neither case were assessments made to understand the nature of the disorder, nor were low-temperature structures determined to explore the possibility of a more ordered phase with possibly a higher Z' number.

Based on prior knowledge, the examination of (1) was made *via* single-crystal X-ray diffraction in the temperature range 110–295 K and cross-polarized light microscopy. The experimental approach includes a crystal morphology study, series of temperature dependences of the cell dimensions in both cooling and heating regimens, a systematic examination of the diffraction pattern, X-ray structure determinations and direct observations of high-quality crystals under a microscope as T varies.

The system (1) is complex, and is characterized by two reversible solid–solid phase transitions and three closely related phases. Quality diffraction patterns can be produced for each individual phase because no significant crystal damage takes place while the system undergoes the two transitions in the cooling and heating regimes. At room temperature the structures of $[M(H_2O)_2(15C5)](HSO_4)_2$ (M = Mn, Ni, Cd) are isomorphous, and the room-temperature phase [hereafter phase (I)] has $Z' = \frac{1}{2}$ and is very disordered. The transition (I) $\Rightarrow$ (II) is characterized by a change in Bravais lattices $C \Rightarrow P$, while Z': $\frac{1}{2} \Rightarrow 1$. The structure of the resulting lower-symmetry phase [hereafter phase (II)] remains very disordered. A second transition occurs at even lower

[1] The geometry of the 15C5 ligand in the $[M(H_2O)(15C5)]^{2+}$ cations (M = Mg, Mn, Fe, Co, Ni, Cu and Zn) is characterized by d(C—C) $\simeq$ 1.50 Å, d(C—O) $\simeq$ 1.43–1.45 Å, (C—C—O) $\simeq$ 105–107° and (C—O—C) $\simeq$ 113–115°.

temperatures; the transition (II) $\Rightarrow$ (III) is accompanied by the change in Z': 1 $\Rightarrow$ 2, and the unit-cell volume is doubled. The structure of the resulting low-temperature phase [hereafter phase (III)] is ordered. Reasons for which structures are either ordered or disordered have been explored. In the three related structures, the hydrogen-bonded network is complicated, and the intermolecular interactions are achieved *via* strong O—H$\cdots$O hydrogen bonds along **a** $\pm$ **b** [phases (I) and (II)] or **a** $\pm$ **b**/2 [phase (III)], **b** and **c**. The role of the counterions in hydrogen bonding has been examined. Crystal packing remains remarkably similar in the phase sequence (I) $\leftrightarrow$ (II) $\leftrightarrow$ (III), but subtle structural differences take place along the face-diagonal directions **a** $\pm$ **b** [phases (I) and (II)] or **a** $\pm$ **b**/2 [phase (III)]. Changes in these structural features are discussed.

2. Experimental

2.1. Synthesis and crystal growth

Crystals were grown by evaporation from an aqueous solution equimolar ($\sim 5 \times 10^{-4}$ mol) in 15C5 and $Ni(SO_4)\cdot 6H_2O$. This synthesis was originally aimed at producing co-crystals containing 15C5, $[Ni(H_2O)_6]^{2+}$ ions, SO_4^{2-} counterions and maybe some uncoordinated water molecules, *e.g.* $[Ni(H_2O)_6](SO_4)\cdot 15C5\cdot xH_2O$ (x = integer or half integer).[2] All crystallization attempts led to green crystals of either the monoclinic or tetragonal polymorphs of $Ni(SO_4)\cdot 6H_2O$ (Angel & Finger, 1988), and no chemical reaction took place between the crown ether and the Ni salt. The green crystals and the unreacted crown ether were subsequently dissolved in a small amount of water; a few drops of 3*M* H_2SO_4 were added afterwards. The pH of the solution remained very low (pH $\leq$ pK_{a2} = 1.9) so that the second dissociation of sulfuric acid was favored in the backward direction. This procedure was aimed at growing crystals that contained $[Ni(H_2O)_6]^{2+}$ ions, HSO_4^- counterions and maybe some water molecules, *e.g.* $[Ni(H_2O)_6](HSO_4)_2\cdot 15C5\cdot xH_2O$ (x = integer or half integer). This last attempt was unsuccessful, and green crystals of $Ni(SO_4)\cdot 6H_2O$ (the two polymorphs) were the sole isolated product. The vial containing the green crystals and the remaining mother liquor was then gently heated from 298 to 373 K, similar to the procedure carried for the synthesis of $[Ni(H_2O)_2(15C5)](NO_3)_2$ (Siegler, Parkin *et al.*, 2008). Near 326 K the green crystals of $Ni(SO_4)\cdot 6H_2O$ decomposed and the color of the remaining solution changed progressively from green to yellow, which hinted at a change in coordination of the Ni^{2+} ion. Yellow crystals of (1) appeared a few minutes after melting of the starting material and grew rapidly. The vial was sealed, and the resulting mixture of yellow crystals and solution was allowed to cool. When removed from the mother liquor, crystals of (1) were found to be moderately moisture sensitive at room temperature; the crystals appeared fragmented and the growth of new green crystallites occurred after an hour or so (see Fig. S-1 of the supplementary material[3]). The resulting green crystals were found to be those of the tetragonal polymorph of $Ni(SO_4)\cdot 6H_2O$. When crystals of (1) were kept within the mother liquor or protected with perfluoropolyalkylether oil, decomposition was much slower (*ca* several days up to weeks).

[2] The compounds $[Ni(H_2O)_6](NO_3)_2\cdot$(15-crown-5)$\cdot nH_2O$ (n = 1, 2) have been successfully isolated (Siegler, Parkin *et al.*, 2008).

2.2. Crystal morphology

Yellow crystals of (1) are tabular and are mostly elongated along the **b*** direction. The largest crystal faces belong to the form {100}, which suggest that crystal growth is favored along the **b*** and **c*** directions (see §3.2.2 for further details). Other important faces correspond to the forms {010} and {001}. The indices are given for the conventional cell of phase (I) ($Cmc2_1$, $Z' = \frac{1}{2}$).[4]

The morphology of one crystal of (1) is depicted in Fig. S-2 of the supplementary material.

2.3. Structure determinations

2.3.1. Generalities. All reflection intensities were measured using a Nonius KappaCCD diffractometer (rotating anode) with graphite-monochromated Mo $K\alpha$ radiation (λ = 0.71073 Å) using the program *COLLECT* (Nonius, 1999). The program *PEAKREF* (Schreurs, 1999) was used to refine the cell dimensions. Data were reduced using the integration program *EvalCCD* (Duisenberg *et al.*, 2003). All structures were solved with *SHELXS*97 and refined on F^2 with *SHELXL*97 (Sheldrick, 2008*a*). Multi-scan semi-empirical absorption corrections based on symmetry-related measurements were applied to all data using *SADABS* Version 2008/1 (Sheldrick, 2008*b*). One good-quality crystal, which was initially placed in a N_2(g) stream in order to prevent crystal decomposition, was used for the whole series of X-ray measurements (*i.e.* three full data sets + measurements of cell constants *versus* T). The data collection temperature was controlled using an Oxford Cryostream 600 (manufactured by Oxford Cryosystems). For the three sets of data, the slices $nk\ell$, $hn\ell$, and hkn, n: 0 $\Rightarrow$ 3 of the reciprocal lattice (hereafter RL) were reconstructed using the routine *PRECESSION* from the program suite *COLLECT* (Nonius, 1999). Careful examinations of these slices showed that the crystal was phase pure. No evidence of non-merohedral twinning was detected. The RL slices have been deposited with the supplementary material.

The H atoms of the 15C5 molecule were placed at calculated positions (instruction AFIX 23 in *SHELXL*97) with isotropic displacement parameters having values 1.2 U_{eq} of the attached C atoms, and were refined with a riding model. The H

[3] Supplementary data for this paper are available from the IUCr electronic archives (Reference: ZB5013). Services for accessing these data are described at the back of the journal.

[4] Sometimes, smaller sloping faces were found to have indices that probably result from several combinations of the **b*** and **c*** vectors. There was however no attempt to index those faces because their indices seem to vary from crystal to crystal. Ideally, crystals of (1) should have the *mm*2 point-group symmetry, but there was no Groth's morphological evidence (Groth, 1906–1919; Curtin & Paul, 1981).

atoms of the water ligands and those of the hydrogen sulfate counterions were found in difference Fourier maps and their positions were restrained such that the O—H distances and the H—O—H angles (water ligands only) had values within accepted ranges [d(O—H) $\simeq$ 0.82–0.84 Å, d(H$\cdots$H) $\simeq$ 1.30 Å so that H—O—H $\simeq$ 104.5° (water ligands only)]. For phases (I) and (II) the H atoms of the hydrogen sulfate ions were placed at calculated positions (AFIX 147 in *SHELXL*97). The atom-numbering schemes of the cations and anions were made consistent in the three reported structures. For phase (III) the RESI instruction available in *SHELXL*97 was used for both cations (residues 1, 2) and anions (residues 3 $\Rightarrow$ 6). For phase (II) this instruction was only used for the anions (residues 1, 2). Displacement ellipsoid plots for the structures of phases (I), (II) and (III) are shown in Fig. 1. The crystallographic data for the three phases of (1) are given in Table 1.

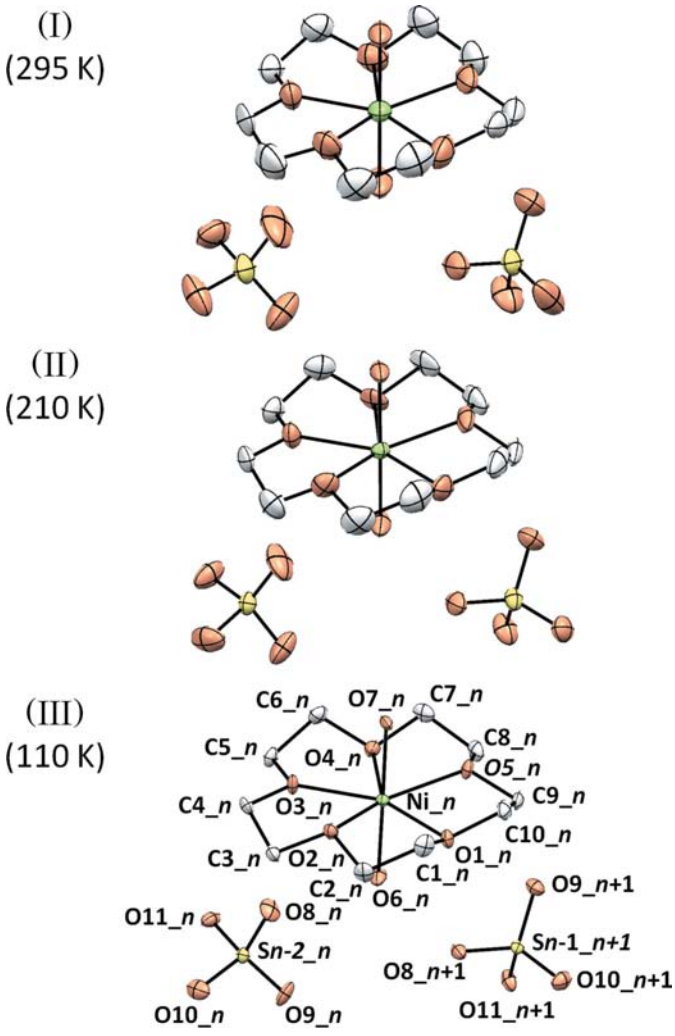

Figure 1
Displacement ellipsoid plots (50% probability level) of one formula unit of (1) for phases (I), (II) and (III) [given at 295 (2), 210 (2) and 110 (2) K]. The atom-numbering scheme is shown. For phase (III) the n variable takes the values 1, 2 for the cations (residue numbers 1, 2) and 3, 5 for the anions (residue numbers 3, 4, 5, 6). Disorder [phases (I) and (II) only] and H atoms are omitted for the sake of clarity.

2.3.2. Phase (I). In the process of determining the unit cell, *DIRAX* (Duisenberg, 1992) found a *C*-centered orthorhombic cell with similar cell constants as those of SIDKEW and SIDKIA (Braga *et al.*, 2007).[5] The structure of phase (I) was solved and refined in $Cmc2_1$ (No. 36) with $Z' = \frac{1}{2}$. There were several warning signs (unusually large ellipsoids, too short or too long C—C, C—O, S—O and S═O bond lengths) suggesting disorder of the formula unit. The cation is found on a crystallographic mirror plane and must be disordered with an occupancy factor of 0.5 because the 15C5 ligand has no mirror symmetry. For the final refinement, the five C—C bond distances were restrained to be similar (SADI instruction); the same set of restraints was applied for the ten C—O_{crown} bond distances. The C and O atoms of the crown ether were restrained to have similar U^{ij} components (SIMU instruction). The Ni ion is split over two sites [Ni1$\cdots$Ni1′ = 0.398 (3) Å] and the occupancy factor of the major component refines to 0.323 (7) [*i.e.* 0.646 (7) $\times$ 0.5 since the cation is located on a mirror plane]. The atomic displacement parameters (hereafter ADPs) of the minor/major Ni^{2+} sites were constrained to be the same (EADP instruction). The O_{water} atoms were treated as ordered in the final model, although the displacement ellipsoids were somewhat elongated (the elongation vector and the vector **Ni1Ni1′** are found along the same direction). The counterion is disordered and the occupancy factor of the major component refines to 0.613 (4). The SIMU instruction was used for all disordered atoms of the counterion, and the minor and major components were restrained to have the same geometry (SAME instruction). Details on the disorder are discussed in §3.

2.3.3. Phase (II). If the crystal is cooled to 210 K,[6] the *C*-centering of the room-temperature cell is lost and the $h + k = 2n + 1$ reflections are not systematically absent, but are found to be systematically weaker than the $h + k = 2n$ reflections (see the reconstructed RL slices given in the supplementary material). A separate Wilson plot (Xia *et al.*, 2001, 2002; bin width 0.02 Å^{-2}) for the classes of odd and even $h + k$ reflections is shown in Fig. 2. The intensity ratio between even and odd $h + k$ reflections for $(\sin\theta/\lambda)^2 < 0.2$ Å^{-2} can be as large as 100, but this ratio decreases to values of $\sim$16–30 when $(\sin\theta/\lambda)^2 > 0.2$ Å^{-2}. The Wilson plot for data collected at 210 K suggests pseudo-*C*-centering with pseudotranslation of $\frac{1}{2}$(**a** + **b**). This intermediate-temperature structure was initially solved using the space group $Pca2_1$ (No. 29), which was later changed to $Pbc2_1$ to facilitate comparison with phase (I). The transformation is given by **a**($Pbc2_1$) = (0 1 0 / 1 0 0 / 0 0 −1)**a**-($Pca2_1$). The cell constants of the $Pca2_1$ cell at 210 K are: a = 7.5069 (3), b = 17.7219 (5), c = 14.7170 (4) Å. The Z' number is

[5] The room-temperature structures SIDKEW and SIDKIA were originally reported in the space group $Ccm2_1$. When the unit cells are reported in $Cmc2_1$ *via* the transformation matrix M = (0 1 0 / 1 0 0 / 0 0 −1), the structures of SIDKEW, SIDKIA and the room-temperature structure of (1) are isomorphous. The cell dimensions of the $Cmc2_1$ cells are: SIDKEW (Mn): a = 18.016 (5), b = 7.418 (3), c = 14.851 (3) Å; SIDKIA (Cd): a = 18.212 (6), b = 7.511 (3), c = 14.920 (6) Å, and phase (I) (Ni): a = 17.8301 (2), b = 7.4833 (1), c = 14.8133 (5) Å.

[6] Phase (II) remains unchanged regardless of how fast (slow) the cooling rate is set during cooling.

Table 1
Experimental details.

For all structures: $C_{10}H_{24}NiO_7{\cdot}2(HO_4S)$, M_r = 509.14. Experiments were carried out with Mo $K\alpha$ radiation using a Nonius KappaCCD diffractometer. Absorption was corrected for by multi-scan methods (*SADABS*; Sheldrick, 2008*b*). H atoms were treated by a mixture of independent and constrained refinement. The absolute structure was obtained using the method of Flack (1983).

	(I)	(II)	(III)
Crystal data			
Crystal system, space group	Orthorhombic, $Cmc2_1$	Orthorhombic, $Pbc2_1$	Orthorhombic, $Pbn2_1$
Temperature (K)	295	210	110
a, b, c (Å)	17.8301 (2), 7.4833 (1), 14.8133 (5)	17.7219 (5), 7.5069 (3), 14.7170 (4)	17.8198 (3), 14.8945 (1), 14.6052 (7)
V (Å^3)	1976.51 (8)	1957.90 (11)	3876.5 (2)
Z, Z'	4, $\frac{1}{2}$	4, 1	8, 2
μ (mm^{-1})	1.26	1.28	1.29
Crystal size (mm)	0.34 × 0.14 × 0.12	0.34 × 0.14 × 0.12	0.34 × 0.14 × 0.12
Data collection			
T_{min}, T_{max}	0.77, 0.86	0.76, 0.86	0.76, 0.86
No. of measured, independent and observed [$I > 2\sigma(I)$] reflections	10 012, 2161, 2017	15 576, 4460, 3394	35 233, 8722, 5725
R_{int}	0.019	0.020	0.032
Refinement			
$R[F^2 > 2\sigma(F^2)]$, $wR(F^2)$, S	0.021, 0.048, 1.10	0.026, 0.069, 1.03	0.031, 0.071, 1.01
No. of reflections	2161	4460	8722
No. of parameters	256	476	541
No. of restraints	296	668	17
$\Delta\rho_{max}$, $\Delta\rho_{min}$ (e Å^{-3})	0.16, −0.22	0.37, −0.26	0.55, −0.42
Flack parameter†	0.004 (12)	−0.004 (11)	0.005 (9)

Computer programs used: *COLLECT* (Nonius, 1999), *PEAKREF* (Schreurs, 1999), *EVALCCD* (Duisenberg *et al.*, 2003), *SHELXS*97, *SHELXL*97 (Sheldrick, 2008*a*), *PLATON* (Spek, 2003). † The crystal class (point group) remains the polar *mm*2 in the sequence (I) ↔ (II) ↔ (III). In the three crystal structures of (1), the absolute direction of the *c* polar axis depends on the orientation of the one-dimensional $\cdots HSO_4^- \cdots H_2O{-}Ni^{2+}{-}OH_2 \cdots HSO_4^- \cdots$ columnar motif with respect to the **c** vector.

1; the cation and the two independent counterions remain disordered similarly to those found in phase (I). The occupancy factor of the major component of the cation refines to 0.689 (3). The two water ligands were treated as ordered in the model. The disorder for the hydrogen sulfate ions was treated similarly to that of phase (I), except that the ADPs for the disordered S and O11 (O11 = hydrogen-bond donor) atoms were constrained to be the same (EADP). The occupancy factors for the two major components of the independent disordered counterions refine to 0.536 (4) and 0.882 (3).

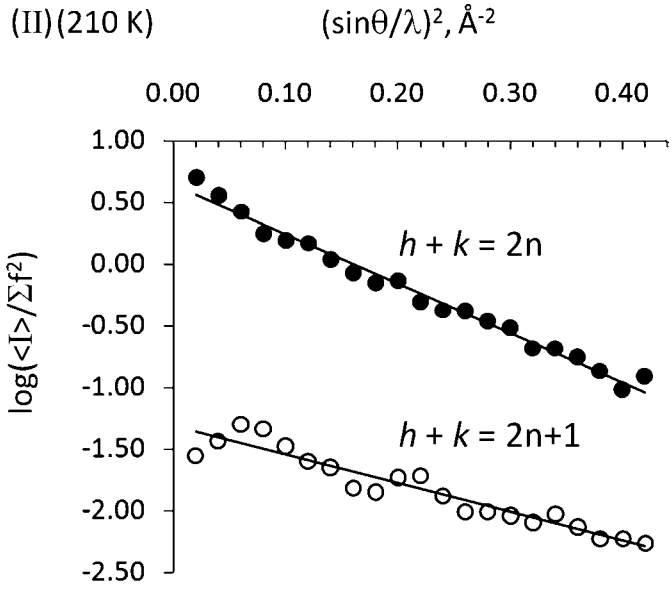

Figure 2
Separate Wilson plot for the odd and even $h + k$ reflections measured at 210 K for phase (II) of (1). Depending on $(\sin\theta/\lambda)^2$, the intensity ratio can take values in the range 16–100. The origin of the vertical scale is arbitrary.

2.3.4. Phase (III). When the crystal was cooled from 210 to 110 K,[7] the diffraction pattern could no longer be indexed correctly with the unit cell of phase (II). The indexing program *DIRAX* (Duisenberg, 1992) found one unit cell twice as large as that of phase (II). The structure was initially solved in the space group $Pna2_1$ (No. 33) with $Z' = 2$, and the cell constants of the $Pna2_1$ cell at 110 K are: a = 14.8945 (1), b = 17.8198 (3), c = 14.6052 (7) Å. This cell was later transformed into the non-standard $Pbn2_1$ cell *via* the transformation (0 1 0 / 1 0 0 / 0 0 −1) to facilitate comparisons with the structures of phases (I) and (II). The two independent formula units are approximately related by a non-space-group translation of $\frac{1}{2}$ (**a** ± **b**/2) (only one of these non-space-group translations is allowed per unit cell). A fit of the two independent formula units [*i.e.* 18 (crown ether) + 10 (counterions) = 28 non-H atoms per formula unit] was made by the program *PLATON* (Spek, 2003), the weighted r.m.s. deviation for the fits was 0.087 Å (see Fig. S-3 of the supplementary material). Despite the observed pseudo-symmetry, the convergence was smooth (the absolute values for the largest correlation matrix elements were no larger than 0.79), and the final refinement was

[7] Phase (III) remains unchanged regardless of how fast (slow) the cooling rate is set during cooling.

straightforward. The structure of phase (III) is ordered. The largest residual peaks are found in the range 0.26–0.48 e Å^{-3}, and are near the hydrogen sulfate ions S2 and S4. These peaks may result from minor librational effects of the anions around the axis S—O11. There is however no clear sign of static disorder of the HSO_4^- counterions because the S—O and S═O bond lengths are normal [d(S—O) $\simeq$ 1.55 Å, d(S═O) $\simeq$ 1.45 Å], and because there are no eccentric features found in the displacement ellipsoids.[8]

2.4. Temperature dependence of the cell dimensions

Three sets of data were collected using an automatic procedure based on the phi/chi cell determination method (Duisenberg *et al.*, 2000). The first set includes reflection intensities (*ca* 800–1500 reflections) that were measured systematically for both cooling and heating regimens between 150 and 270 K at ± 10 K intervals (cooling/heating rates were set to ± 4 K min^{-1}, see Table S-1 for data) in order to derive the overall profiles of the cell dimensions *versus* T (*i.e.* a, b, c and the volume per formula unit V/Z *versus* T). Two additional sets (*ca* 700–1200 reflections) were collected in the temperature ranges 186–222 and 242–278 K at ± 4 K intervals (cooling/heating rates were set to ± 2 K min^{-1}), and were aimed at locating with more precision the two cooling and heating transitions (see Tables S-2 and S-3 for data). The two V/Z *versus* T profiles are shown in Fig. 3.

2.5. Cross-polarized light microscopy

Microphotographs of one high-quality crystal of (1) (see Fig. 4) were taken under cross-polarized light using an Olympus BX41 research-grade microscope with a 5× microscope objective lens and a CCD video camera (ColorView IIIu, Soft Imaging System GmbH). A 75 W Xenon lamp was used for illumination. The crystal was protected against moisture by immersion in perfluoropolyalkylether oil in order to prevent fast decomposition. The crystal was subsequently cooled and heated in an *in situ* cell (FTIR 600, Linkam Scientific Instruments) equipped with a temperature controller (Linkam TMS 93). The precision of these temperature measurements was ±1 K, and the cooling/heating rates were set to ± 2 K min^{-1}. This experimental approach was used to observe the crystal of (1) passing through the transition (I) ↔ (II). Attempts to follow the same procedure for the lower-temperature transition (II) ↔ (III) failed because the oil chosen for this experiment had a melting point near 253 K. Solidification of the oil causes several major problems (*e.g.* difficulty to focus, blurry images), which made interpretation of the results unacceptable.

[8] Before the final refinement was carried out, the occupancy factors for all atoms of the counterions S2 and S4 were refined as free variables (FVAR), and their values refined to 1.004 (2) and 0.991 (2), which suggested there is no disorder. These occupancy factors were subsequently fixed to 1 in the final refinement.

3. Results and discussion

3.1. Phase transitions

3.1.1. Order of the phase transitions. Precise measurements of the volume per formula unit V/Z *versus* T were aimed at locating within a few degrees (approximately ± 2 K) the two transition temperatures $T_{I \leftrightarrow II}$ and $T_{II \leftrightarrow III}$ in both cooling and heating regimes. The cooling transition temperatures $T_{II \Leftarrow I}$ and $T_{III \Leftarrow II}$ are found at 252 and 192 K, whereas the heating transition temperatures $T_{III \Rightarrow II}$ and $T_{II \Rightarrow I}$ are found at 200 and 264 K. The lower- and higher-temperature transitions (II) ↔ (III) and (I) ↔ (II) are characterized by small $|\Delta V/Z|$ of 1.62 (4) and 0.63 (5) Å^3, and estimated hysteresis of 8 (2) and 12 (2) K. The two transitions are first order since the V/Z *versus* T profiles show discontinuities and significant hysteresis near the two transition points.

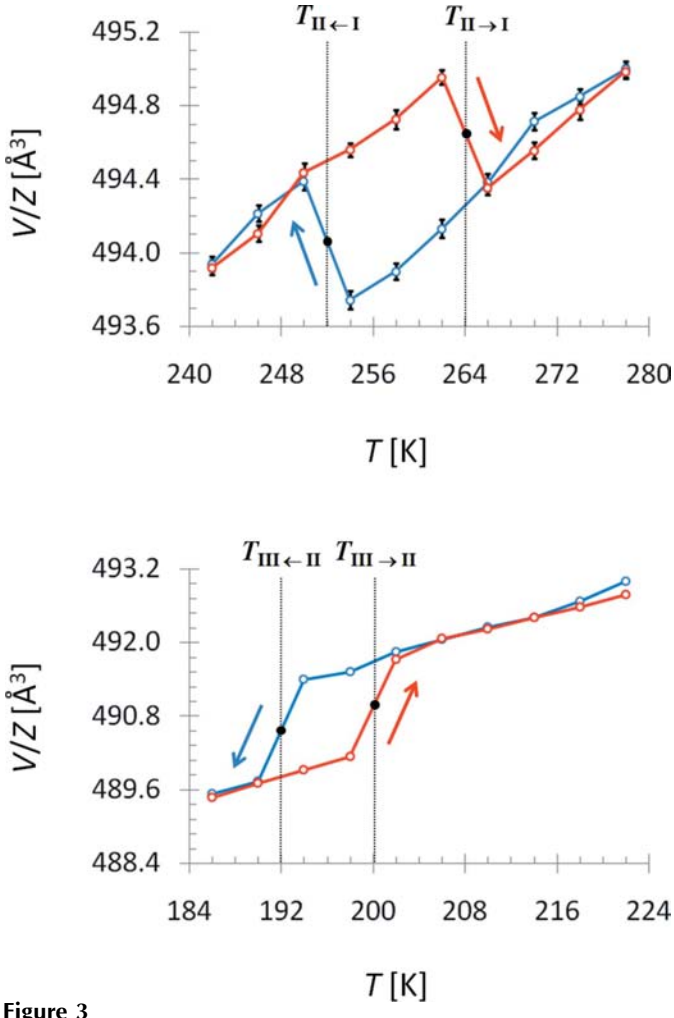

Figure 3
Plots of the volume per formula unit V/Z (Å^3) *versus* T (K). Values of V/Z are measured for the solid–solid phase transitions (I) ↔ (II) (T range: 242–278 K) and (II) ↔ (III) (T range: 186–222 K) at ± 4 K for both cooling (blue lines) and heating (red lines) regimens. Discontinuities in V/Z are found for both transitions. The positions of the vertical thin lines give the estimated temperatures for which the discontinuities occur. Error bars associated with V/Z are shown. For the transition (II) ↔ (III), the error bars are not significant compared with the vertical axis scale. This figure is in color in the electronic version of this paper.

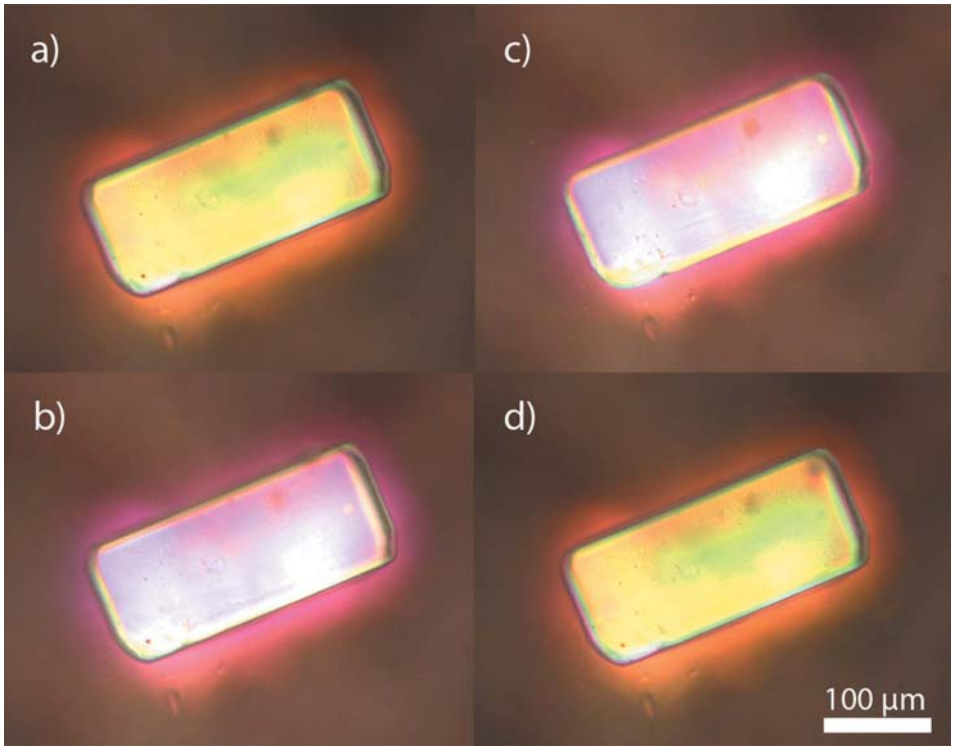

Figure 4
Microphotographs of one crystal of (1) taken under cross-polarized light during cooling from 254 K (*a*) to 252 K (*b*) and during heating from 263 K (*c*) to 265 K (*d*). The spontaneous change in interference color takes place as the crystal undergoes the transition (I) ↔ (II).

Direct observations of crystals of (1) under a cross-polarized light microscope in the T range 250−270 K showed a spontaneous change in interference color between 254 and 252 K on cooling, and between 263 and 265 K on heating. Both optical microscopy and X-ray diffraction techniques give very similar transition temperatures and hysteresis widths for the transition (I) ↔ (II).

3.1.2. Directionality of structural changes in the sequence (I) ↔ (II) ↔ (III). The supergroup–subgroup relationship for (I) ↔ (II) is defined by the Bravais relationship $C \leftrightarrow P$ associated with Z': $\frac{1}{2} \leftrightarrow 1$. The absolute values for the differences in cell constants associated with (I) ↔ (II) are largest for $|\Delta a|$ (*ca* 0.10 Å), intermediate for $|\Delta b|$ (*ca* 0.04 Å) and smallest for $|\Delta c|$ (*ca* 0.02 Å). On the cooling transition (I) ⇒ (II), the $\Delta V/Z$ value is positive (because the increase in the *b* and *c* axes outweighs the decrease in the *a* axis), which is rather unusual.

The lower-temperature transition (II) ↔ (III) is of the order–disorder type, and is associated with Z': 1 ↔ 2, and with the doubling of the *b* axis. The $Z' = 2$ structure [phase (III)] is an ordered modulated variant of the simpler, but disordered $Z' = 1$ structure [phase (II)]. The structure of phase (III) is pseudosymmetric, and contains pairs of homochiral (but crystallographically independent) cations that are related by the pseudotranslation of $\frac{1}{2}$ (**a** ± **b**/2).[9] The absolute values for the differences in cell constants associated with (II) ↔ (III) are largest for $|\Delta a|$ (*ca* 0.09 Å), and $|\Delta b'|$ [*ca* 0.06 Å; $b' = b$ for phase (II) and $b' = b/2$ for phase (III)], and smallest for $|\Delta c|$ (*ca* 0.02 Å). On the cooling transition (II) ⇒ (III), the $\Delta V/Z$ value is negative (because the decrease in the *b* and *c* axes outweighs the increase in the *a* axis).[10]

The change in Bravais lattice for (I) ↔ (II) and the occurrence of pseudosymmetry for phase (III) suggest that important structural changes are driven along the face-diagonal directions **a** ± **b** [phases (I) and (II)] and **a** ± **b**/2 [phase)III)]. The $\frac{1}{2}$ ($a + b'$) *versus* T profile shows discontinuities for both transitions (see Fig. S-4 of the supplementary material).

3.2. Structural features

3.2.1. Ni—O distances. The small ionic radius of the Ni^{2+} ion (0.69 Å; Shannon, 1976) and its chemical preference for octahedral geometry may compel the metal ion to occupy more than one position within the cavity of the 15C5 ligand. Large discrepancies in the Ni—O_{crown} bond lengths are found for (1). In the low-temperature structure [phase (III)],[11] the two crystallographically independent cations have four Ni—O_{crown} distances in the range 2.05−2.25 Å and one Ni—O_{crown} distance in the range 2.50–2.65 Å. The uneven distribution of the Ni—O_{crown} suggests that the metal ion is strongly coordinated by only four of the five O_{crown} atoms (*i.e.* O1, O2, O3 and O5).[12] The metal centers are ordered in the low-temperature structure of (1).

The average Ni—O_{water} bond lengths for the compounds $[Ni(H_2O)_2(15C5)](X)_2$ ($X = HSO_4^-, NO_3^-$) are the same within the standard error [*i.e.* 1.998 (5) and 1.990 (3) Å; the values in parentheses correspond to the standard deviations of the

[9] The directions **a** ± **b**/2 in the structure of phase (III) are equivalent to the face-diagonal directions **a** ± **b** in the structures of phases (I) and (II).

[10] The significant changes in the *a* and *b* axes may result from some structural rearrangements of the cations/anions along the face-diagonal directions **a** ± **b** [phases (I) and (II)] and **a** ± **b**/2 [phase (III); see §3.3 for further details].

[11] These bond lengths are more accurately measured in the structure of phase (III) because the amplitude of vibration in the crystal lattice is significantly reduced at lower temperature.

[12] Similar observations have been made for the related compound $[Ni(H_2O)2(15C5)](NO_3)_2$ (Siegler, Parkin *et al.*, 2008).

mean]. The Ni—O_{crown} and Ni—O_{water} distances for the three phases of (1) are summarized in Table 2.

3.2.2. O—H···O hydrogen bonds. The hydrogen-bond interactions found in the structures of (1) are achieved *via* six donors [*i.e.* four H atoms of the two axial water ligands and two H atoms of the two HSO_4^- counterions] and six acceptors (*i.e.* six O_{anion} atoms of the two HSO_4^- counterions), which lead to the existence of six strong O—H···O hydrogen bonds per formula unit (*i.e.* four O_{water}—H···O_{anion} and two O_{anion}—H···O_{anion}). We are mostly concerned with the ordered phase (III) because the positions of the H atoms are better resolved in the low-temperature structure.

One important hydrogen-bonding motif is found between the cations and the counterions along [001], and its graph-set notation (Etter *et al.*, 1990) is $R_4^3(10)$. Each water ligand (O6 and O7) is donor to two independent hydrogen sulfate ions in two O_{water}—H···O_{anion} bonds. Each counterion bridges two successive cations. Half of the time there are two acceptors per counterion (the atoms O8 and O9 for the counterions S1 and S3) in two O_{water}—H···O_{anion} bonds, but the rest of the time there is one bifurcated acceptor per counterion (the atom O8 for the counterions S2 and S4) in two O_{water}—H···O_{anion} bonds. The remaining acceptor O9 for the counterions S2 and S4 may participate in weaker C_{crown}—H···O_{anion} bonds to counterbalance the lack of strong acceptors (C_{crown}···O_{anion} distances are found in the range 3.071−3.216 Å, the individual s.u.s are 0.003−0.004 Å). The eight independent O_{water}···O_{anion} distances are found in the range 2.671−2.748 Å with O_{water}—H—O_{anion} angles found within 158−176° (the individual s.u.s are 0.003 Å and 3°, respectively). The $R_4^3(10)$ motif allows the building of one-dimensional columns ···HSO_4^-···H_2O—Ni^{2+}—OH_2···HSO_4^-··· (see Fig. 5*a*).

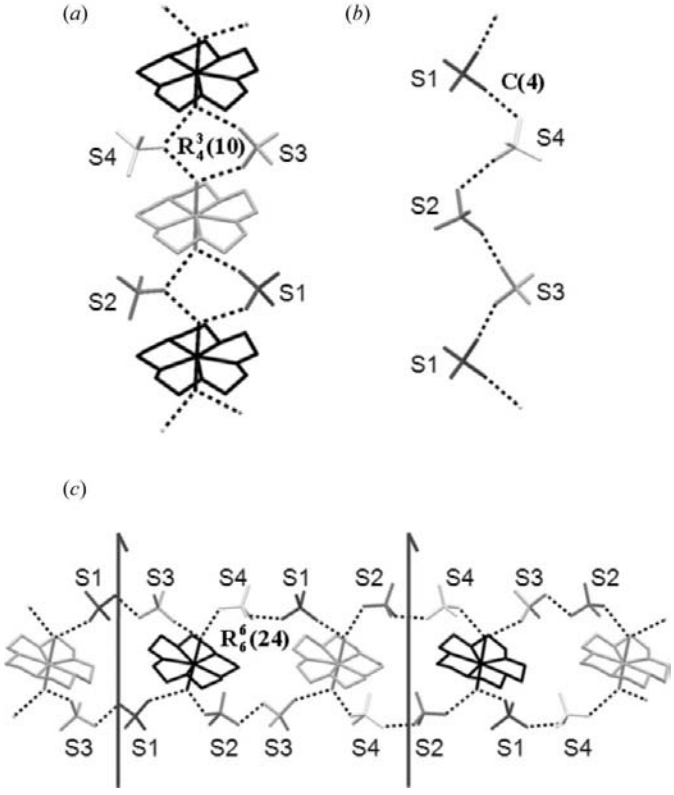

Figure 5
(*a*) Drawing showing the $R_4^3(10)$ motif found along [001] [phase (III)]. The top and bottom crown molecules are related by a translation of *c*. Each water ligand (O_{water}) makes two O_{water}—H···O_{anion} hydrogen bonds. This motif is asymmetric because two anions (S2 and S4) make bifurcated hydrogen bonds, whereas the two others (S1 and S3) participate in two non-bifurcated hydrogen bonds. (*b*) Drawing showing the *C*(4) motif found along [010] [phase (III)]. The top and bottom counterions are related by a translation of *b*. Anions are both donors and acceptors in strong O_{anion}—H···O_{anion} hydrogen bonds. (*c*) Drawing showing the $R_6^6(24)$ motif found along [1 $\pm\frac{1}{2}$ 0] [phase (III)]. There are four independent $R_6^6(24)$ motifs: two motifs are exclusively built of two S1—O—H···O—S3 or two S2—O—H···O—S4 bridges, and two motifs are built of one S4—O—H···O—S1 and one S3—O—H···O—S1 bridge. The positions of the 2_1 screw axes are shown. The crystallographically independent parts are colored differently for drawings (*a*), (*b*) and (*c*).

Table 2
Ni—O distances (Å) for the cations $[Ni(H_2O)_2(15C5)]^{2+}$ in (1).

These distances are given for the structures of phases (I), (II) and (III), determined at 295, 210 and 90 K, respectively. The Ni—O distances for phases (I) and (II) are only given for the major component of the disorder.

	(I)	(II)	(III)	
			Residue (1)	Residue (2)
Ni—O_{crown}				
Ni—O1	2.117 (12)	2.090 (5)	2.0766 (19)	2.064 (2)
Ni—O2	2.043 (11)	2.097 (5)	2.0746 (19)	2.129 (2)
Ni—O3	2.157 (14)	2.158 (5)	2.147 (2)	2.183 (2)
Ni—O4	2.515 (5)	2.534 (4)	2.607 (2)	2.566 (2)
Ni—O5	2.239 (13)	2.201 (6)	2.203 (2)	2.175 (2)
Ni—O_{water}				
Ni—O6	2.002 (3)	1.998 (2)	2.005 (2)	1.998 (2)
Ni—O7	1.996 (3)	1.993 (2)	1.996 (2)	1.994 (2)

Another motif is found between the counterions along [010], and its graph-set notation is *C*(4). The counterions have one donor (O11—H11) and one acceptor (O10) atom. These hydrogen bonds are the strongest in the crystal, and the four independent O_{anion}···O_{anion} distances are found in the range 2.565−2.583 Å with O_{anion}—H—O_{anion} angles found within 158−166° (the individual s.u.s are 0.003 Å and 3°). The *C*(4) motif generates infinite one-dimensional ribbons (see Fig. 5*b*).

The third motif results from a combination of O_{water}—H···O_{anion} and O_{anion}—H···O_{anion} hydrogen bonds along [1 $\pm\frac{1}{2}$ 0], and its graph-set notation is $R_6^6(24)$. Successive cations in the $R_6^6(24)$ motif are interlinked *via* a set of two S—O—H···O—S bridges (see Fig. 5*c*). The $R_6^6(24)$ motif varies along [1 $\pm\frac{1}{2}$ 0]. There is one motif exclusively built of S1—O—H···O—S3 bridges, and another motif exclusively built of S2—O—H···O—S4 bridges. The bridges are related by 2_1 axes in these two motifs. The remaining motifs contains one S3—O—H···O—S2 and one S1—O—H···O—S4 bridge, and there is no symmetry-imposed relationships between the bridges.

All O_{water}···O_{anion} and O_{anion}···O_{anion} hydrogen bonds are summarized in Table S-4 of the supplementary material.

3.2.3. Pseudosymmetry and disorder. In the structure of phase (III) ($Pbn2_1$, Z' = 2), pseudosymmetry occurs in the

hydrogen-bonded layers parallel to (001). Every second pair of cations found along the **a** ± **b**/2 directions is conformationally homochiral,[13] and these pairs are always related by a pseudotranslation of $\frac{1}{2}(a \pm b/2)$. The set of counterions S1 and S3 (or S2 and S4) are also related by the same pseudotranslation vectors. All cations lie on *b* glide planes, and half of the counterions lie on *n* glide planes. The combination of *n* glide planes ⊥ to **b** with the pseudotranslation vectors $\frac{1}{2}(\mathbf{a} \pm \mathbf{b}/2)$ generates four non-crystallographically pseudo *c* glide planes ⊥ to **b** located at the *y* positions 1/8, 3/8, 5/8 and 7/8, and the interplanar distance is *b*/4 (see Fig. S5 of the supplementary material).[14] Neighboring hydrogen-bonded layers ⊥ to **c** are related by 2_1 axes and *n* glide planes, and there is no required symmetry-imposed disorder in the $Pbn2_1$ structure.

After completion of the transition (III) ⇒ (II), the *b* axis is shortened by a factor of two in the structure of phase (II) ($Pbc2_1$, $Z' = 1$), and the pseudo-*c* glide planes in the $Pbn2_1$ cell become true *c* glide planes in the $Pbc2_1$ cell. The pseudotranslation vectors are $\frac{1}{2}(\mathbf{a} \pm \mathbf{b})$, and the cell of phase (II) is pseudo-*C*-centered. Pseudo-mirror planes ⊥ to **a** are found at $x = \frac{1}{4}$ and $\frac{3}{4}$. In the $Pbc2_1$ structure, neither the cations nor the counterions lie on *b* glide planes. An ordered $Pbc2_1$ structure would require the following conditions:

(i) successive cations along **a** ± **b** are conformational enantiomers,

(ii) successive cations along **b** are homochiral,

(iii) the $R_6^6(24)$ motifs are exclusively built of either S1—O—H···O—S3 or S2—O—H···O—S4 bridges.

None of these conditions are fulfilled in the $Pbn2_1$ structure. The symmetry relationship of the $Pbn2_1 \Rightarrow Pbc2_1$ transition then requires disorder of the cations in the $Pbc2_1$ structure, which must result from the non-superimposition of the conformational enantiomers *R* and *S*. Similarly, disorder of the counterions must result from the non-superimposition of the bifurcated and the non-bifurcated orientations.

After completion of the transition (II) ⇒ (I), the translation vectors $\frac{1}{2}(\mathbf{a} \pm \mathbf{b})$ are found in the cell of phase (I) ($Cmc2_1$, $Z' = \frac{1}{2}$). Disorder remains very similar in the $Pbc2_1$ and $Cmc2_1$ structures, but the cations occupy sites of statistical mirror symmetry in the latter structure.

3.3. Structural differences along *a* ± *b* and *a* ± *b*/2 directions in the sequence (I) ↔ (II) ↔ (III)

3.3.1. Enantiomeric alternation pattern. In the structures of the three phases of (1), conformational enantiomers *R* and *S* are related by glide-plane symmetry.

Structural differences between the three phases of (1) are found within rows of cations along the directions **a** ± **b**/2 [phase (III)] and **a** ± **b** [phases (I) and (II); see Fig. 6]. Along these directions, successive cations are connected by a set of two S—O—H···O—S bridges that are found in the $R_6^6(24)$ motif. In the low-temperature structure [phase (III)], the cations fail to alternate once every two opportunities, and there is the pattern of alternation of conformational enantiomers *R R S S R R S S* within a row parallel to **a** ± **b**/2. Alternation fails when pairs of homochiral cations are related by pseudotranslation of $\frac{1}{2}$ (**a** ± **b**/2). Alternation is always achieved when the two S—O—H···O—S bridges of the $R_6^6(24)$ motif are related by 2_1 axes, and non-alternation occurs when there is no symmetry relationship between the bridges. In the intermediate- and room-temperature structures [phases (II) and (I)], there is no long-range enantiomeric alternation pattern because the cations are disordered. The pattern would be perfect if one of the two components of the disorder was ignored.

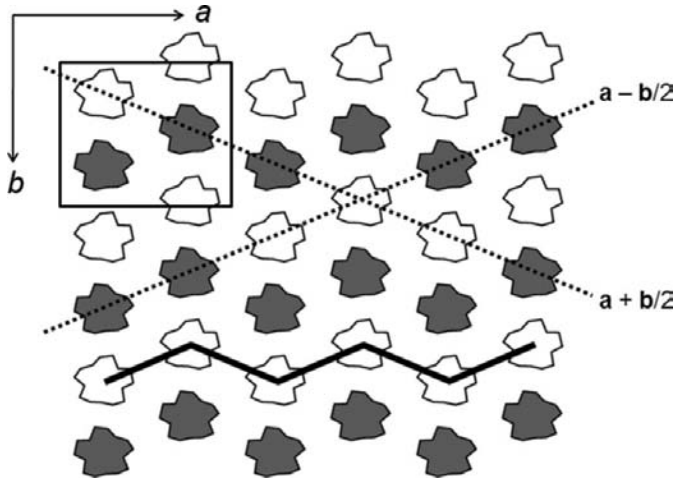

Figure 6
Drawing of one (001) layer of the $Pbn2_1$ structure ($0 \le z \le \frac{1}{2}$). The white and dark gray-colored cations are conformational enantiomers. Every second pair of cations are conformationally homochiral along the **a** ± **b**/2 directions, and two homochiral cations are related by pseudotranslation of $\frac{1}{2}(a \pm b/2)$. Triangular patterns of homochiral cations propagate along the **a** direction because pseudotranslation occurs successively along the **a** + **b**/2 and **a** − **b**/2 directions from one cell to another. The counterions and H atoms are omitted for the sake of clarity.

3.3.2. Ni···Ni, Ni—O_{water}···O_{water}—Ni distances and S—O—H···O—S bridges. In the sequence (I) ↔ (II) ↔ (III) the average Ni···Ni distance remains similar [*i.e.* 9.668, 9.623 and 9.657 Å for phases (I), (II) and (III), respectively], whereas the individual Ni···Ni distances vary significantly from one phase to another. In the low-temperature structure [phase (III)], there are successively two shorter (9.593 and 9.572 Å) and two longer (9.713 and 9.749 Å) Ni···Ni distances.[15] The deviations of the Ni···Ni distances from the average value are as large as ± 0.09 Å. In the intermediate-temperature structure [phase (II)], the number of independent Ni···Ni distances has been reduced to two. The shorter and longer Ni···Ni distances are respectively 9.597 and 9.649 Å; the deviations of

[13] The cation $[M(H_2O)_2(15C5)]^{2+}$ possesses an axis of chirality, and therefore has two conformational enantiomers (see Hao *et al.*, 2005; Hao, Siegler *et al.*, 2005, for further details).

[14] The atomic coordinates (*x*, *y*, *z*) are transformed *via* the pseudotranslation $\frac{1}{2}$ (**a** − **b**/2) into $(x + \frac{1}{2}, y - \frac{1}{4}, z)$, which are subsequently transformed *via n* glide plane symmetry (to **b**) into $(x + 1, \frac{1}{2} + \frac{1}{4} - y, z + \frac{1}{2})$. This set of coordinates is equivalent to $(x, \frac{1}{2} - y, z + \frac{1}{2}) + (0, \frac{1}{4}, 0)$, which indicates the presence of **c** glide planes separated by **b**/4.

[15] Since the pattern of alternation of conformational enantiomers is *R R S S R R S S* along the **a** ± **b**/2 directions, then there are one shorter and one longer *R R* (or *S S*) non-alternations. The same observations are found for the *R S* (or *S R*) alternations.

these distances from their average value are no larger than ± 0.03 Å. In the room-temperature structure, the Ni···Ni spacing becomes even because of the space group translation $\frac{1}{2}(a + b)$.

The distances Ni—O_{water}···O_{water}—Ni of two consecutive cations that are connected by the S—O—H···O—S bridges also show some large discrepancies. The Ni···Ni distances always lie between one shorter and one longer Ni—O_{water}···O_{water}—Ni distances. In the structure of phase (III) the max–min difference in Ni—O_{water}···O_{water}—Ni distances (hereafter, $\Delta d_{max-min}$) is no larger than 0.095 Å for the non-alternations *R R* and *S S*, whereas $\Delta d_{max-min}$ can be as large as 0.243 Å for the alternations *R S* and *S R*. The $\Delta d_{max-min}$ is minimized significantly (0.041 Å) in the structure of phase (II), and is zero in the structure of phase (I).

While the distances Ni—O_{water}···O_{water}—Ni vary significantly, the HSO_4^- counterions can adopt different orientations in order to offset the uneven spacing between successive cations along the **a** ± **b** and **a** ± **b**/2 directions. Changes in the hydrogen bonds S—O—H···O—S may be minimized in the crystal lattice. The two favorable orientations are 'b' and 'nb' [*i.e.* bifurcated and non-bifurcated orientation in the $R_4^3(10)$ motif, respectively].[16] These orientations may complicate the packing arrangement (see Fig. S-6 of the supplementary material).[17]

3.4. $Z' > 1$?

Some general thoughts on the existence of $Z' > 1$ structures have been put forward in the literature over the last decade (Steiner, 2000; Steed, 2003; Desiraju, 2007; Anderson & Steed, 2007; Steed & Atwood, 2009). Structures with $Z' > 1$ commonly show signs of structural complexity – *e.g.* cooperative effects between optimization of intermolecular interactions (owing to the presence of highly directional O—H···O hydrogen bonds) and optimal packing requirements, pseudosymmetry, modulation, and packing frustration due to the awkward molecular shape.

The low-temperature structure of (1) [phase (III)] is one example for which structural complexity occurs and for which $Z' > 1$. This structure includes a complicated set of strong O—H···O hydrogen bonds showing highly directional preferences along the **a** ± **b**/2, **b** and **c** directions. Along the latter direction, the optimization of hydrogen bonds fails because 25% of the O_{anion} atoms are not acceptors in O—H···O interactions. Bifurcated hydrogen bonds are preferred even though there is potentially an equal number of hydrogen-bond donors and acceptors. The asymmetrical $R_4^3(10)$ motif is then preferred to the symmetrical $R_4^4(10)$ motif, and contributes to the building of columns for which the counterions bridge the cations along **c**. The asymmetrical nature of the cations[18] may favor the formation of columns built of hydrogen-bonded motifs with a preference for asymmetrical properties (Exarchos *et al.*, 2001).

Approximate symmetry elements are found in the structure of phase (III). Pseudotranslation occurs when conformational enantiomers *R* and *S* fail to alternate along **a** ± **b**/2. The nature of the S—O—H···O—S bridges found in the four independent $R_6^6(24)$ motifs (along **a** ± **b**/2) seems to be critical in the existence of alternations *R S* (or *S R*) and non-alternations *R R* (or *S S*). The arrangement of these bridges can vary because counterions adopt the bifurcated and non-bifurcated orientations, which are found in the asymmetrical $R_4^3(10)$ motif. Such motifs are likely to complicate the crystal packing, and one possible outcome would be a $Z' > 1$ structure.

4. Summary

A system of three related phases has been discovered for the compound $[Ni(H_2O)_2(15C5)](HSO_4)_2$ between 295 and 110 K. This system is an example for which lowering the temperature induces a rise in Z' values. The sequence (I) ↔ (II) ↔ (III) is characterized by the Z' change, $\frac{1}{2} \leftrightarrow 1 \leftrightarrow 2$, which is accompanied by a symmetry breakdown and by the ordering in the crystal lattice while the thermal motion effects are reduced. Such systems are ideal for investigating structure relationships occurring through solid–solid phase transitions because crystal damage remains negligible and because packing arrangements for each individual phase can be easily compared.

This work was supported by Utrecht University and by the Council for Chemical Sciences of The Netherlands Organization for Scientific Research (CW-NWO). This work was also supported by the Dutch National Science Foundation VENI subsidy (ES).

References

Allen, F. H. (2002). *Acta Cryst.* B**58**, 380–388.
Anderson, K. M. & Steed, J. W. (2007). *CrystEngComm*, **9**, 328–330.
Angel, R. J. & Finger, L. W. (1988). *Acta Cryst.* C**44**, 1869–1873.
Braga, D., Gandolfi, M., Lusi, M., Polito, M., Rubini, K. & Grepioni, F. (2007). *Cryst. Growth Des.* **7**, 919–924.
Curtin, D. Y. & Paul, I. C. (1981). *Chem. Rev.* **81**, 525–541.
Desiraju, G. R. (2007). *CrystEngComm*, **9**, 91–92.
Duisenberg, A. J. M. (1992). *J. Appl. Cryst.* **25**, 92–96.
Duisenberg, A. J. M., Hooft, R. W. W., Schreurs, A. M. M. & Kroon, J. (2000). *J. Appl. Cryst.* **33**, 893–898.
Duisenberg, A. J. M., Kroon-Batenburg, L. M. J. & Schreurs, A. M. M. (2003). *J. Appl. Cryst.* **36**, 220–229.
Etter, M. C., MacDonald, J. C. & Bernstein, J. (1990). *Acta Cryst.* B**46**, 256–262.
Exarchos, G., Robinson, S. D. & Steed, J. W. (2001). *Polyhedron*, **20**, 2951–2963.
Flack, H. D. (1983). *Acta Cryst.* A**39**, 876–881.

[16] The counterions of this motif participate in the S—O—H···O—S bridges.
[17] In the structure of phase (III) the bridges can have three different geometries. The three possibilities of bridges are b···b, nb···nb, b···nb (or nb···b). For the non-alternations *R R* and *S S*, two independent b···nb (or nb···b) bridges are found. For the alternations *R S* and *S R*, there are either two equivalent b···b or two equivalent nb···nb bridges that are related by 21 axes. In the structures of phases (I) and (II) the counterions are disordered and so are the bridges.
[18] The 15C5 ligand is asymmetric because it contains an odd number of C—C—O fragments.

Groth, P. (1906–1919). *Chemische Kristallographie.* Leipzig: Verlag von Wilhelm Engelmann.
Hao, X., Parkin, S. & Brock, C. P. (2005). *Acta Cryst.* B**61**, 675–688.
Hao, X., Siegler, M. A., Parkin, S. & Brock, C. P. (2005). *Cryst. Growth Des.* **5**, 2225–2232.
Nonius (1999). *Collect.* Nonius BV, Delft, The Netherlands.
Schreurs, A. M. M. (1999). *PEAKREF.* University of Utrecht, The Netherlands.
Shannon, R. D. (1976). *Acta Cryst.* A**32**, 751–767.
Sheldrick, G. M. (2008*a*). *Acta Cryst.* A**64**, 112–122.
Sheldrick, G. M. (2008*b*). *SADABS*, Version 2008/1. University of Göttingen, Germany.
Siegler, M. A. (2007). PhD Dissertation, University of Kentucky, http://lib.uky.edu/ETD/ukychem2007d00664/dissertationMASiegler.pdf.
Siegler, M. A., Hao, X., Parkin, S. & Brock, C. P. (2008). *Acta Cryst.* B**64**, 738–749.
Siegler, M. A., Hao, X., Parkin, S. & Brock, C. P. (2010). In preparation.
Siegler, M. A., Parkin, S. & Brock, C. P. (2010). In preparation.
Siegler, M. A., Parkin, S., Selegue, J. P. & Brock, C. P. (2008). *Acta Cryst.* B**64**, 725–737.
Spek, A. L. (2003). *J. Appl. Cryst.* **36**, 7–13.
Steed, J. W. (2003). *CrystEngComm*, **5**, 169–179.
Steed, J. W. & Atwood, J. L. (2009). *Supramolecular Chemistry*, 2nd ed. New York: Wiley.
Steiner, T. (2000). *Acta Cryst.* B**56**, 673–676.
Xia, A., Selegue, J. P., Carrillo, A., Patrick, B. O., Parkin, S. & Brock, C. P. (2001). *Acta Cryst.* B**57**, 507–516.
Xia, A., Selegue, J. P., Carrillo, A., Patrick, B. O., Parkin, S. & Brock, C. P. (2002). *Acta Cryst.* B**58**, 565.